Kinematic Characteristics of PKIKP and its Derived Phases Based on the IASP91 Earth Model

G. Wenqi[1], W. Youxue[2,*], and Y. Songping[1]

[1]College of Earth Sciences, Guilin University of Technology, Guilin, China.

[2]Institute of Urban Underground Space and Energy Studies, The Chinese University of Hong Kong, Shenzhen,China.

Corresponding author: W. Youxue (uxue.wang@glut.edu.cn)

Key Points:

- PKIKP and its derived phases
- Upper mantle transition zone
- Velocity discontinuity
- Kinematic characteristics

Abstract

Since PKIKP is a teleseismic phase with small angle arrived at station, almost vertical to the surface, it is an important phase for establishing the earth's structure interior, including its derived phases reflected from discontinuity boundaries at the 410 km and 660 km in the upper mantle transitional zone. In this paper, based on the IASP91 Earth velocity model and raytracing technique, the kinematic characteristics of the PKIKP and its derived phases are numerically simulated and analyzed. The results show that the arrivals of the pairs of P_4PKIKP and PKIKPP_4, pP_4PKIKP and pPKIKPP_4, P_6PKIKP and PKIKPP_6, pP_6PKIKP and pPKIKPP_6 derived from PKIKP are coincided each other, respectively, enhancing the energies for phase identification. The phases pPKIKP, pPKIKPP_4, and pPKIKPP_6 arrivals are parallel to each other and phases PKIKP, PKIKPP_4, and PKIKPP_6 arrivals also are parallel to each other for the events with different source depths, and that the time differences between PKIKPP_4 and PKIKP, PKIKPP_6 and PKIKP always parallel each other and independent of the source depth. When the velocity discontinuity of the upper mantle transitional zone is inclined toward the increasing epicenter distance direction, the travel time of phases PKIKPP_4 or PKIKPP_6 will increase with distance increasing; Conversely, the travel time will decrease with distance increasing.

1 Introduction

The upper mantle transition zone with its discontinuities is an important part in studying the deep structure within the earth (Dziewonski and Anderson, 1981; Flanagan and Shearer, 1998; Shearer, 1995; Tibi and Wiens, 2005). Near the depths of 410 km and 660 km in the upper mantle, there are obvious discontinuities in the seismic velocities, and the material between the two discontinuities constitutes the upper mantle transition zone, and that these two discontinuities have been observed and confirmed by many seismic observations in a global scale[*Shearer and Flanagan, 1999; Benz and Vidale, 1993; Wang and Niu, 2010; Day, 2013; Zhang et al., 2019*]. Usually, the discontinuities mainly are studied by using SS or PP waves [*Deuss et al., 2006; Lee and Grand, 1996*], ScS multiples [*Bagley et al., 2013; Courtier and Revenaugh, 2006, 2007; Katzman et al., 1998; Revenaugh and Jordan, 1991; Wang et al., 2017*], and receiver functions [*Agius et al., 2017; Ai et al., 2003; Wei and Chen, 2016*], etc.

However, as a teleseismic phase, PKIKP (also known as PKPdf), the ray path of which almost through the crust, upper mantle, lower mantle, outer core and inner core [*Larry, 2001*], has a clearly visible energy in many strong earthquakes. The phase is important to shape the structure of the transitional zone in upper mantle, especially the radial velocity variation, and its ray arrives at station with a small angle, almost vertical to the earth's surface. If the PKIKP phase is reflected from discontinuities at the depth of 410km and 660km in the upper mantle beneath the source or station to produce a reflection sub-ray, noted as P_4 and P_6, respectively, and some derived phases are then generated, such as P_4PKIKP, P_6PKIKP, pP_4PKIKP, pP_6PKIKP phases reflected from the discontinuities beneath event source, PKIKPP_4, PKIKPP_6, pPKIKPP_4, pPKIKPP_6 phases reflected from the discontinuities beneath receiver station, and mixed phases P_4PKIKPP_4, P_6PKIKPP_6, pP_4PKIKPP_4, pP_6PKIKPP_6 reflected from the discontinuities beneath both source and station. At the same time, due to the deep propagation through core, PKIKP and its derived phases arrive station almost vertical to the surface [*Gutenberg, 1960; Cleary and Hales, 1971*], so that they should be the best data for establishing the velocity structure of the Earth's interior without any transformation, especially epicentral distance beyond 160 degree.

Based on existing standard Earth models [e.g., PREM model, *Dziewonski and Anderson 1981*; IASP91 model, *Kennett and Engdahl 1991*; AK135 model, *Kennett, 1995*] and using ray tracing [*Steck et al., 1998; Bijwaard and Spakman, 1999; Keyser et al., 2002; Zhao and Lei, 2004; Vidale and Helmberger, 1988; Vidale, 1990; Rawlinson and Sambridge, 2004*], the travel times or the differential travel times of the phases can be used to investigate the radial velocity structure of the Earth's interior.

In this paper, the kinematic characteristics of these phases and their interrelationships will be discussed based upon the IASP91 Earth velocity model and by using numerical modeling technique.

2 Kinematic characteristics of PKIKP and its derived phases

For a strong teleseismic earthquake, the ray paths of PKIKP and its derived phases within the Earth's interior are show in Figure 1, and the rays arrive station with a small angle, almost vertical to the earth's surface.

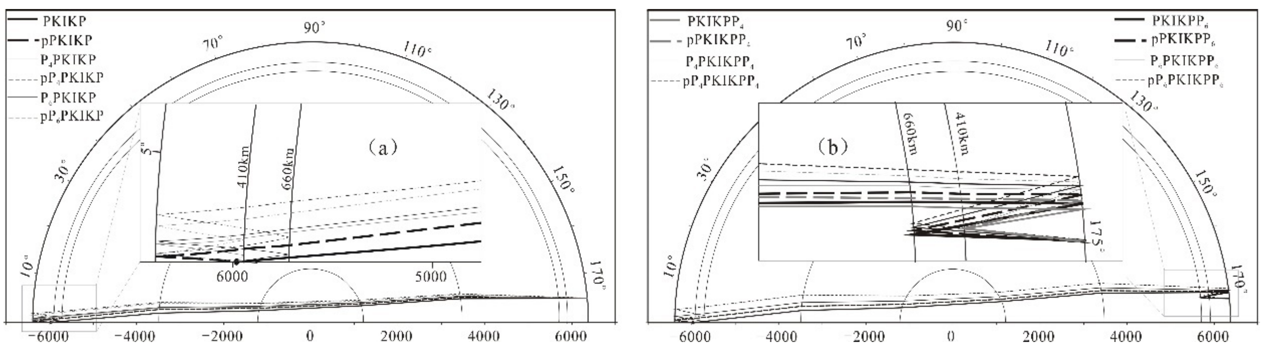

Figure 1. Ray paths of PKIKP and its derived phases in the Earth's interior

(a and b correspond to the reflection from the discontinuity beneath source and station, respectively)

Based on the IASP91 Earth velocity model, the travel times and ray paths of PKIKP and its derived phases were calculated for two cases by using ray tracing [*Jiang et al., 2019*] with a ray tracing accuracy of 0.01s (table 1, and table 2). The first case sets the distance range of 160° ~180° with step 5 degree and source depth of 300km (Tabe 1), and second case fixes the station at 175 degree to change the source depth from 20km to 600km (Tabe 2), and the trave times are shown in Figure 2.

Table 1a. The travel times and angles out of surface for PKIKP and its derived phases

(Source at depth of 300 km)

distance(deg.)	160		165		170		175		180	
phase	travel time(s)	Angle (deg.)	travel time(s)	Angle (deg.)	travel time(s)	Angle (deg.)	travel time(s)	Angle (deg.)	travel time(s)	Angle (deg.)
PKIKP	1162.56	3.76	1167.55	2.89	1171.17	1.95	1173.37	0.98	1174.09	0.00
pPKIKP	1238.22	3.87	1243.32	2.99	1247.03	2.03	1249.28	1.02	1250.02	0.00
P_4PKIKP	1263.03	3.61	1268.17	2.78	1271.92	1.88	1274.19	0.95	1274.94	0.00
P_6PKIKP	1313.86	3.98	1319.14	3.08	1322.99	2.10	1325.33	1.06	1326.10	0.00

pP$_4$PKIKP	1338.68	3.72	1343.94	2.87	1347.78	1.95	1350.10	0.98	1350.87	0.00
pP$_6$PKIKP	1389.49	4.11	1394.89	3.20	1398.84	2.18	1401.24	1.10	1402.03	0.00
PKIKPP$_4$	1263.03	3.61	1268.17	2.78	1271.92	1.88	1274.19	0.95	1274.94	0.00
PKIKPP$_6$	1313.86	3.98	1319.14	3.09	1322.99	2.10	1325.33	1.06	1326.10	0.00
pPKIKPP$_4$	1338.68	3.72	1343.94	2.87	1347.78	1.95	1350.11	0.98	1350.87	0.00
pPKIKPP$_6$	1389.49	4.11	1394.89	3.20	1398.84	2.18	1401.24	1.10	1402.03	0.00
P$_4$PKIKPP$_4$	1363.48	3.72	1368.79	2.87	1372.66	1.95	1375.02	0.98	1375.79	0.00
P$_6$PKIKPP$_6$	1465.08	4.22	1470.67	3.30	1474.78	2.25	1477.28	1.14	1478.11	0.00
pP$_4$PKIKPP$_4$	1439.11	3.84	1444.54	2.98	1448.51	2.02	1450.93	1.02	1451.73	0.00
pP$_6$PKIKPP$_6$	1540.68	4.36	1546.41	3.43	1550.62	2.35	1553.19	1.19	1554.04	0.00

Table 1b. The travel times for the source at different depth (station at distance of 175°)

depth(km) / travel time(s)	20.00	100.00	200.00	300.00	600.00
PKIKP	1207.88	1197.49	1185.21	1173.37	1141.28
pPKIKP	1214.77	1225.16	1237.44	1249.28	1281.36
P$_4$PKIKP	1308.70	1298.31	1286.03	1274.19	--
pP$_4$PKIKP	1315.59	1325.98	1338.26	1350.10	--
P$_6$PKIKP	1359.84	1349.45	1337.17	1325.33	1293.24
pP$_6$PKIKP	1366.73	1377.12	1389.40	1401.24	1433.32
PKIKPP$_4$	1308.70	1298.31	1286.03	1274.19	--
pPKIKPP$_4$	1315.59	1325.98	1338.26	1350.10	--
P$_4$PKIKPP$_4$	1409.53	1399.14	1386.86	1375.02	--
pP$_4$PKIKPP$_4$	1416.43	1426.81	1439.09	1450.93	--
PKIKPP$_6$	1359.84	1349.45	1337.17	1325.33	1293.24
pPKIKPP$_6$	1366.73	1377.12	1389.40	1401.24	1433.32
P$_6$PKIKPP$_6$	1511.79	1501.41	1489.12	1477.28	1445.20
pP$_6$PKIKPP$_6$	1518.68	1529.07	1541.36	1553.19	1585.27

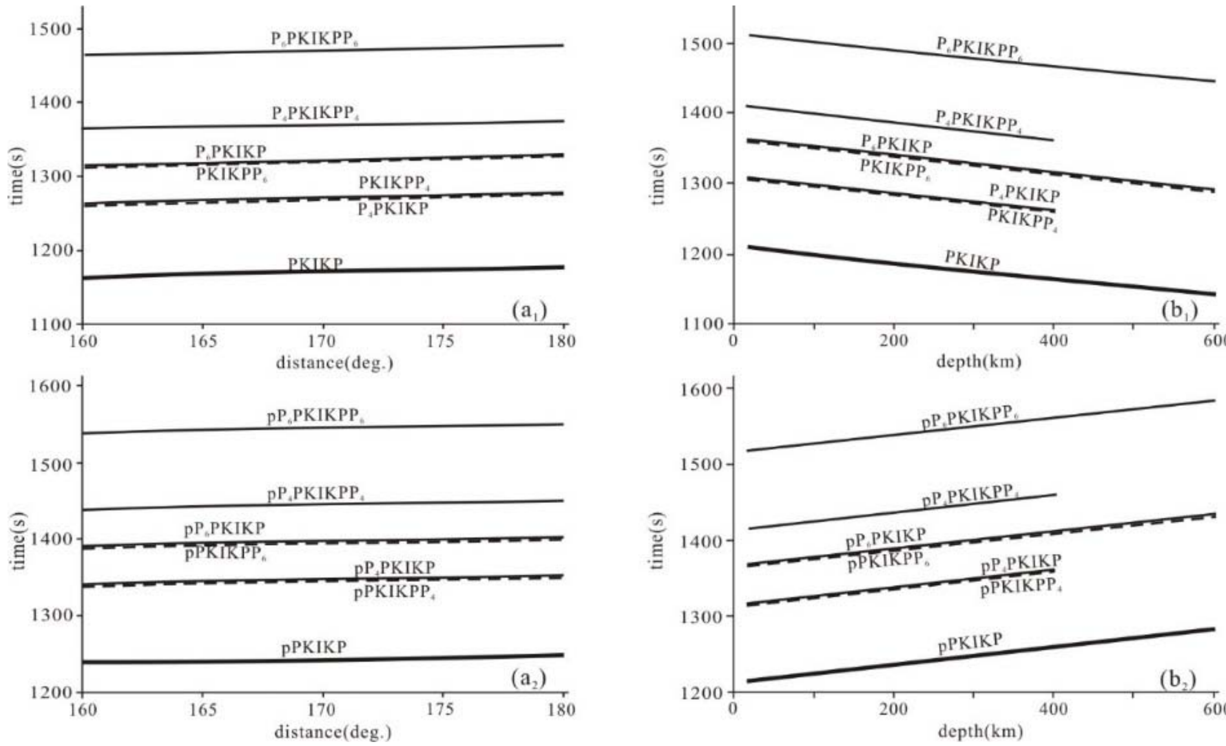

Figure 2. travel times of PKIKP and its derived phases

(a and b are corresponding to first case and second case, respectively)

From the numerical modeling results (Table 1 and Figure 2) for PKIKP and its derived phases, it can be seen that for an earthquake at a depth of 300 km, the travel time increases with distance increasing regardless of the presence of p phase (Figure 2a). For a fixed station at distance of 175 degree, the travel time for each phase decreases with source depth increasing when there is no p phase occurred (Figure 2b1), otherwise, the travel time for each phase increases with source depth increasing when p phase occurred and a series of derived phases are formed (Figure 2b2). Also, it can be seen from Table 1 and Figure 3 that all angles that rays arrive at station are less than 4.5 degree and decreases with distance increasing.

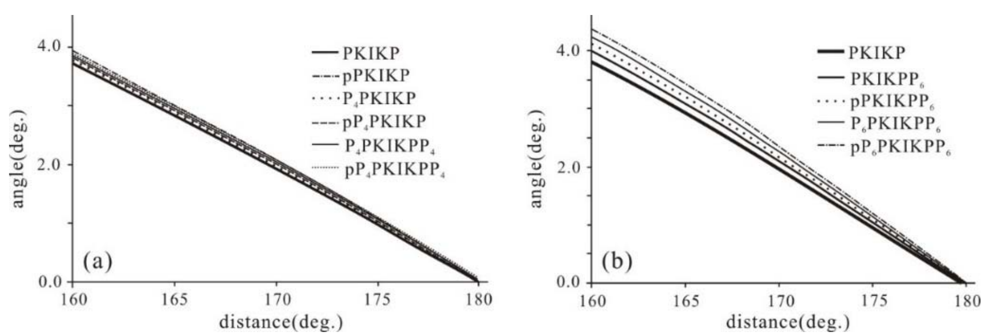

Figure 3. Variation of angles rays arrive at station with distance

(a and b correspond to the reflection from 410 and 660km discontinuity, respectively)

Table 2a. The kinematic features of phase P_4PKIKP and PKIKPP_4, P_6PKIKP and PKIKPP_6 for source at depth of 300km

distance (deg.) / time/difference (s)	160.00	165.00	170.00	175.00	180.00
P_4PKIKP	1263.03	1268.17	1271.92	1274.19	1274.94
PKIKPP_4	1263.03	1268.17	1271.92	1274.19	1274.94
P_4PKIKP- PKIKPP_4	<0.005	<0.005	<0.005	<0.005	<0.005
P_6PKIKP	1313.86	1319.14	1322.99	1325.33	1326.10
PKIKPP_6	1313.86	1319.14	1322.99	1325.33	1326.10
P_6PKIKP- PKIKPP_6	<0.005	<0.005	<0.005	<0.005	<0.005

Table 2b. The kinematic features of phases P_4PKIKP and PKIKPP_4, P_6PKIKP and PKIKPP_6 for fixed station at distance of 175 degree

depth(km) / time/difference (s)	20.00	100.00	200.00	300.00	600.00
P_4PKIKP	1308.70	1298.31	1286.03	1274.19	--
PKIKPP_4	1308.70	1298.31	1286.03	1274.19	--
P_4PKIKP- PKIKPP_4	<0.005	<0.005	<0.005	<0.005	--
P_6PKIKP	1359.84	1349.45	1337.17	1325.33	1293.24
PKIKPP_6	1359.84	1349.45	1337.17	1325.33	1293.24
P_6PKIKP- PKIKPP_6	<0.005	<0.005	<0.005	<0.005	<0.005

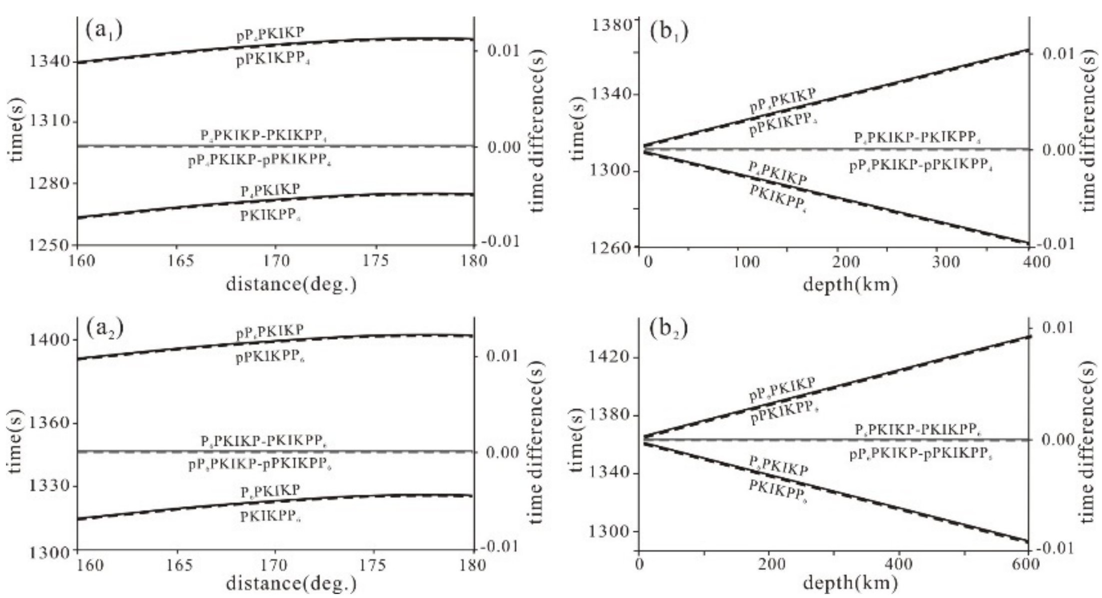

Figure 4. The Kinematic features of corresponding phase pairs

(a and b are corresponding to the first case and second case, respectively)

For the same source at depth of 300km, the travel time difference between P_4PKIKP and PKIKPP_4, pP_4PKIKP and pPKIKPP_4, P_6PKIKP and PKIKPP_6, pP_6PKIKP and pPKIKPP_6 are less than 0.005s (Table 2a and Figure 4a), which is much smaller than the ray tracing precision (0.01s), and it can be considered that the phases for each phase pair arrives same time at station.

On the other hand, for a fixed station at distance of 175 degree (Table 2b and Figure 4b), when the source depth varies from 20km to 600km, the travel times of the derived phases above are exactly the same. Therefore, the derived phases for each phase pair of P_4PKIKP and $PKIKPP_4$, pP_4PKIKP and $pPKIKPP_4$, P_6PKIKP and $PKIKPP_6$, pP_6PKIKP and $pPKIKPP_6$ arrive at the same time, respectively. This case implies that the energy of each pairs will be double to make the phases stronger to be identified easily. For discussion convenient, we only use the one phase of each pairs, $PKIKPP_4$ and $pPKIKPP_4$, $pPKIKPP_6$ and $PKIKPP_6$, and ignore others of $PKIKPP_4$ and $pPKIKPP_4$, $pPKIKPP_6$ and $PKIKPP_6$ in the later discussion.

Table 3a. Travel time differences relative to time the from the source of 200km (received at same distance of 175 degree)

depth(km) / time difference(s)	20.00	100.00	300.00	600.00
PKIKP	22.67	12.28	-11.85	-43.93
pPKIKP	-22.67	-12.28	11.85	43.93
$PKIKPP_4$	22.67	12.28	-11.85	--
$pPKIKPP_4$	-22.67	-12.28	11.85	--
$PKIKPP_6$	22.67	12.28	-11.85	-43.93
$pPKIKPP_6$	-22.67	-12.28	11.85	43.93

Table 3b. time difference between derived phases and PKIKP for different source depths

depth(km) / time difference(s)	20.00	100.00	200.00	300.00	600.00
$PKIKPP_4$-PKIKP	100.82	100.82	100.82	100.82	--
$PKIKPP_6$-PKIKP	151.96	151.96	151.96	151.96	151.96
pPKIKP-PKIKP	6.89	27.67	52.23	75.91	140.08
$pPKIKPP_4$-PKIKP	107.71	128.49	153.05	176.73	--
$pPKIKPP_6$-PKIKP	158.85	179.63	204.19	227.87	292.04
$PKIKPP_6$- $PKIKPP_4$	51.14	51.14	51.14	51.14	51.14
$pPKIKPP_4$-pPKIKP	100.82	100.82	100.82	100.82	--
pPKIKPP6-pPKIKP	151.96	151.96	151.96	151.96	151.96

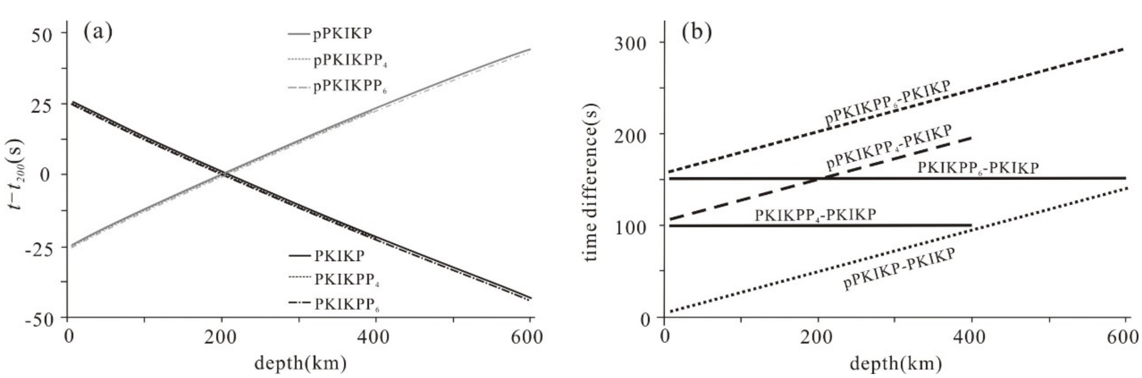

Figure 5. Kinematic characteristics of PKIKP and its derived phases for different source depth at distance of 175 degree

If all trave times from different source at distance of 175 degree in Table 2 subtract the travel time of corresponding phase produced by the source at depth of 200km to form a Table 3a and Figure 5a, which indicate that the time differences for PKIKP, $PKIKPP_4$, and $PKIKPP_6$ phases decreases with source depth increasing, and the time differences for pPKIKP, $pPKIKPP_4$, and $pPKIKPP_6$ phases increases with source depth increasing.

Meanwhile, if all trave times from different source at distance of 175 degree in Table 2 subtract the travel time of PKIKP to form a Table 3b and Figure 5b, two group paralleling lines, one group includes pPKIKP, $pPKIKPP_4$, and $pPKIKPP_6$ which parallels each other and the time difference increases with the source depth increasing; and another group of PKIKP, $PKIKPP_4$, and $PKIKPP_6$ phases not only parallels each other but also the time differences have no variation with constants, the phase $PKIKPP_4$ at 100.82s and the phase $PKIKPP_6$ at 151.96s. This strongly suggests that the time difference between the phase $PKIKPP_4$, $PKIKPP_6$ and PKIKP respectively has no relationship with the source depth, i.e., if setting the arrivals of PKIKP as zero, the phases pPKIKP, $pPKIKPP_4$, $pPKIKPP_6$ parallels each other, and $PKIKPP_4$ and $PKIKPP_6$ will keep constant of 100.82s and 151.96s, respectively.

According to the feature between the phases PKIKP, $PKIKPP_4$ and $PKIKPP_6$, all data from different events with PKIKP, $PKIKPP_4$ and $PKIKPP_6$ can be put together to form a longer align to use as a databank to shape the topography of the discontinuities of 410 km and 610 km in the upper mantle transition zone.

Usually, the discontinuity of 410km or 660km in upper mantle transitional zone is not horizontal. Supposing an inclined discontinuity of 660km keep 660km at a distance of 167 degree for a source at depth 400km, and then let the discontinuity incline 8 degree toward distance increasing direction and reversed direction with the same dip angle, we calculate the travel time from 165 degree to 170 degree for PKIKP and $PKIKPP_6$, and take $dt=t_{PKIKPP6}-t_{PKIKP}$ calculations (Table 4 and Figure 6).

Table 4 The time differences between PKIKPP6 and PKIKP

dip (deg.)	Distance (deg.)	165.00	166.00	167.00	168.00	169.00	170.00
8.00	*dt*(s)	145.01	148.05	151.10	154.15	157.18	160.23
	boundary depth(km)	628.74	644.37	660.00	675.63	691.25	706.88
0.00	*dt*(s)	152.99	152.90	152.80	152.70	152.62	152.54
	boundary depth(km)	660.00	660.00	660.00	660.00	660.00	660.00
-8.00	*dt*(s)	156.53	153.31	150.10	146.90	143.71	140.53
	boundary depth(km)	691.26	675.63	660.00	644.37	628.75	613.12

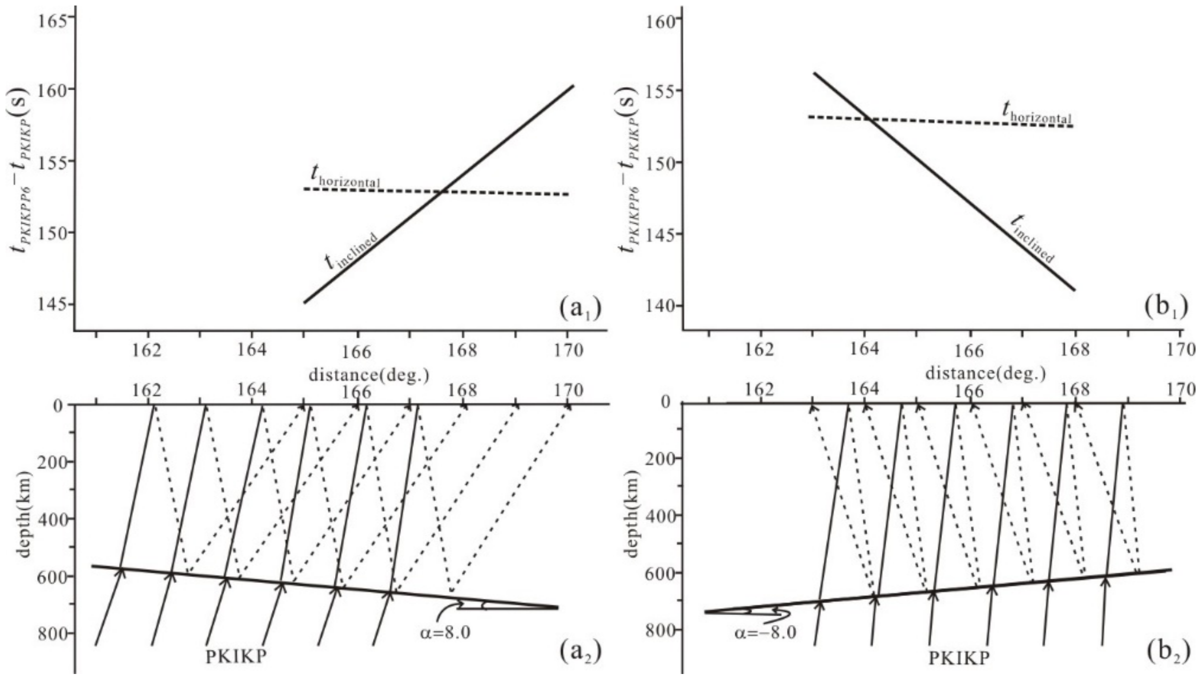

Figure 6 Dip discontinuity of 660km and the travel times of $PKIKPP_6$ and PKIKP

The numerical modeling results (Table 4, Figure 6) show that the time differences between $PKIKPP_6$ and PKIKP increases with the distance increasing when the discontinuity dips toward the direction of distance increasing, and decreases with the distance increasing when dipping toward the direction of distance decreasing. Similarly, the discontinuity of 410 km also shares the same feature. Therefore, the occurrence of the discontinuity, either 410km or 660km can be shaped by the feature of the time differences of $PKIKPP_4$-PKIKP and $PKIKPP_6$-PKIKP, respectively.

3 Conclusions

Based upon the IASP91 Earth velocity model and ray tracing technique, this paper discusses the kinematic characteristics for PKIKP and its derived phases, either along distance align or variation with the source depth. After analyzing and discussion, the conclusion can be given as following:

(1) for each of the phase among the pairs P_4PKIKP and $PKIKPP_4$, pP_4PKIKP and $pPKIKPP_4$, P_6PKIKP and $PKIKPP_6$, pP_6PKIKP and $pPKIKPP_6$, the travel time is equal each other, so the waveform of the phase can be enhanced for identification easily.

(2) for different source depths, the arrivals of PKIKP, $PKIKPP_4$ and $PKIKPP_6$ phases decrease with source depth increasing and are parallel to each other, whereas increase with source depth increasing for pPKIKP, $pPKIKPP_4$, and $pPKIKPP_6$ phases and are parallel to each other.

(3) arrivals of $PKIKPP_4$ and $PKIKPP_6$ from different source depths are both parallel to the PKIKP, and their travel time relative to PKIKP are independent of the source depth.

(4) if setting the arrival time of PKIKP as zero, all data from different events with PKIKP, $PKIKPP_4$ and $PKIKPP_6$ can be put together to form a longer align to shape the topography of the discontinuities of transition zone in the upper mantle.

(5) When the discontinuity of the transition zone in the upper mantle inclines toward the direction of distance increasing, the travel time will decrease with distance increasing, and will increase with distance increasing when dipping toward the direction of distance increasing.

Acknowledgments

- The authors declare no conflict of interest.
- This work was supported by the Guangxi Natural Science Foundation Key Fund Project (2016GXNSFDA380014).

Open Research

The code used in this article is written by the author and has been uploaded as an .exe executable file.

References

Agius, M. R., Rychert, C. A., Harmon, N., & Laske, G. (2017). Mapping the mantle transition zone beneath Hawaii from Ps receiver functions: Evidence for a hot plume and cold mantle downwellings. *Earth and Planetary Science Letters*, *474*, 226-236. doi:10.1016/j.epsl.2017.06.033.

Ai, Y., Zheng, T., Xu, W., He, Y., & Dong, D. (2003). A complex 660 km discontinuity beneath northeast China. *Earth and Planetary Science Letters, 212(1-2)*, 63-71. doi:10.1016/S0012-821X(03)00266-8.

Benz H. M., & Vidale J. E.(1993), Sharpness of upper-mantle discontinuities determined from high-frequency reflections. *Nature*, *365* : 147. doi:10.1038/365147a0.

Bagley, B., Courtier, A. M., & Revenaugh, J. (2013). Seismic shear wave reflectivity structure of the mantle beneath northeast China and the northwest Pacific. *Journal of Geophysical Research: Solid Earth*, *118*(10), 5417-5427. doi:10.1002/jgrb.50385.

Bijwaard, H., & Spakman, W. (1999). Fast kinematic ray tracing of first-and later-arriving global seismic phases. *Geophysical Journal International*, *139*(2), 359-369. doi:10.1046/j.1365-246x.1999.00950.x.

Courtier, A. M., & Revenaugh, J. (2006). A water-rich transition zone beneath the eastern United States and Gulf of Mexico from multiple ScS reverberations. *Geophysical Monograph-American Geophysical Union*, *168*, 181. doi:10.1029/168GM14.

Courtier, A. M., & Revenaugh, J. (2007). Deep upper-mantle melting beneath the Tasman and Coral Seas detected with multiple ScS reverberations. *Earth and Planetary Science Letters*, *259*(1-2), 66-76. doi:10.1016/j.epsl.2007.04.027.

Cleary, J. R., & Hales, A. L. (1971). PKIKP times and S station anomalies. *Journal of Geophysical Research*, *76*(29), 7249-7259. doi:10.1029/JB076i029p07249.

Dziewonski A. M., & Anderson D. L. (1981), Preliminary reference earth model. *Phys Earth Planet Int, 25(4)*, 297-356. doi:10.1016/0031-9201(81)90046-7.

Day E. A., & Deuss A.(2013), Reconciling PP and P′ P′ precursor observations of a complex 660 km seismic discontinuity. *Geophysical Journal International*, *194(2)*, 834-838. doi:10.1093/gji/ggt122.

Deuss, A., Redfern, S. A., Chambers, K., & Woodhouse, J. H. (2006). The nature of the 660-kilometer discontinuity in Earth's mantle from global seismic observations of PP precursors. *Science*, *311(5758)*, 198-201. doi: 10.1126/science.1120020.

Dziewonski, A. M., & Anderson, D. L. (1981). Preliminary reference Earth model. *Physics of the earth and planetary interiors*, *25*(4), 297-356. doi:10.1016/0031-9201(81)90046-7.

Flanagan M. P., & Shearer P. M. (1998). Global mapping of topography on transition zone velocity discontinuities by stacking SS precursors. *Journal of Geophysical Research: Solid Earth*, *103(B2)*, 2673-2692. doi:10.1029/97JB03212.

Gutenberg, B. (1960). PKIKP and pseudo-PKIKP phases at distances of less than 140°. *Geophysical Journal International*, *3*(2), 250-257. doi:10.1111/j.1365-246X.1960.tb00393.x.

Jiang, C., Wang, Y., Xiong, B., Ren, Q., Hu, J., Gao, W., ... & Zhuo, X. (2020). Numerical modeling of global seismic phases and its application in seismic phase identification. *Earthquake Science*, *32*(2), 72-79. doi: 10.29382/eqs-2019-0072-04.

Kenntt, B. L. N., & Engdahl, E. R. (1991). Travel times for global earthquake location and phase association. *Geophysical Journal International*, *105*, 429-465. doi: 10.1111/j.1365-246X.1991.tb06724.x.

Kennett, B. L., Engdahl, E. R., & Buland, R. (1995). Constraints on seismic velocities in the Earth from traveltimes. *Geophysical Journal International*, *122*(1), 108-124. doi:10.1111/j.1365-246X.1995.tb03540.x.

Lee, D. K., & Grand, S. P. (1996). Depth of the upper mantle discontinuities beneath the East Pacific Rise. *Geophysical research letters*, *23(23)*, 3369-3372. doi:10.1029/96GL03103.

Revenaugh, J., & Jordan, T. H. (1991). Mantle layering from ScS reverberations: 3. The upper mantle. *Journal of Geophysical Research: Solid Earth*, *96*(B12), 19781-19810. doi:10.1029/91JB01487.

Ruff, L. J. (2001). PKIKP... and Those Mysterious Precursors. *Seismological Research Letters*, *72*(1), 80-81. doi:10.1785/gssrl.72.1.80.

Shearer P. M. (1995), Seismic studies of the upper mantle and transition zone.*Reviews of Geophysics.,33(s1)*, 321-324. doi:10.1029/95RG00186.

Steck, L. K., Thurber, C. H., Fehler, M. C., Lutter, W. J., Roberts, P. M., Baldridge, W. S., ... & Sessions, R. (1998). Crust and upper mantle P wave velocity structure beneath Valles caldera, New Mexico: results from the Jemez teleseismic tomography experiment. *Journal of Geophysical Research: Solid Earth*, *103*(B10), 24301-24320. doi:10.1029/98JB00750.

Katzman, R., Zhao, L., & Jordan, T. H. (1998). High-resolution, two-dimensional vertical tomography of the central Pacific mantle using ScS reverberations and frequency-dependent travel times. *Journal of Geophysical Research: Solid Earth*, *103*(B8), 17933-17971. doi:10.1029/98JB00504.

Keyser, M., Ritter, J. R., & Jordan, M. (2002). 3D shear-wave velocity structure of the Eifel plume, Germany. *Earth and Planetary Science Letters*, *203*(1), 59-82. doi:10.1016/S0012-821X(02)00861-0.

Rawlinson, N., & Sambridge, M. (2004). Multiple reflection and transmission phases in complex layered media using a multistage fast marching method. *Geophysics, 69(5)*, 1338-1350. doi:10.1190/1.1801950.

Shearer P. M., & Flanagan M. P. (1999), Seismic Velocity and Density Jumps Across the 410- and 660-Kilometer Discontinuities. *Science*, *285(5433)*, 1545-1548. doi:10.1126/science.285.5433.1545.

Tibi R., & Wiens D. A. (2005), Detailed structure and sharpness of upper mantle discontinuities in the Tonga subduction zone from regional broadband arrays. *Journal of Geophysical Research: Solid Earth*, *110(B6)*, 3433. doi:10.1029/2004JB003433.

Vidale, J. E. (1990). Finite-difference calculation of traveltimes in three dimensions. *Geophysics*, *55*(5), 521-526. doi:10.1190/1.1442863.

Vidale, J. E., & Helmberger, D. V. (1988). Elastic finite-difference modeling of the 1971 San Fernando, California earthquake. *Bulletin of the Seismological Society of America*, *78*(1), 122-141. doi:10.1785/BSSA0780010122.

Wang B., & Niu F. (2010), A broad 660 km discontinuity beneath northeast China revealed by dense regional seismic networks in China. *Journal of Geophysical Research: Solid Earth*, *115(B6)*, 6608. doi:10.1029/2009JB006608.

Wang, X., Li, J., & Chen, Q. F. (2017). Topography of the 410 km and 660 km discontinuities beneath the Japan Sea and adjacent regions by analysis of multiple-ScS waves. J*ournal of Geophysical Research: Solid Earth, 122(2)*, 1264-1283. doi:10.1002/2016JB013357.

Wei, S. S., & Chen, Y. J. (2016). Seismic evidence of the Hainan mantle plume by receiver function analysis in southern China. *Geophysical Research Letters*, *43*(17), 8978-8985. doi:10.1002/2016GL069513.

Zhang, M., Sun, D., Wang, Y., & Wu, Z. (2019). Fine structure of the 660-km discontinuity beneath southeastern China. *Geophysical Research Letters*, *46(13)*, 7304-7314. doi:10.1029/2019GL082639.

Zhao, D., & Lei, J. (2004). Seismic ray path variations in a 3D global velocity model. *Physics of the Earth and Planetary Interiors*, *141*(3), 153-166. doi:10.1016/j.pepi.2003.11.010.